Sensors and Actuators B 249 (2017) 715–724

Contents lists available at ScienceDirect

Sensors and Actuators B: Chemical

journal homepage: www.elsevier.com/locate/snb

Ultrasensitive and low detection limit of nitrogen dioxide gas sensor based on flower-like ZnO hierarchical nanostructure modified by reduced graphene oxide

Jie Liu, Shan Li, Bo Zhang, Yan Xiao, Yuan Gao*, Qiuyue Yang, Yinglin Wang, Geyu Lu*

State Key Laboratory on Integrated Optoelectronics, College of Electronic Science and Engineering, Jilin University, 2699 Qianjin Street, Changchun 130012, China

ARTICLE INFO

Article history:
Received 13 October 2016
Received in revised form 27 April 2017
Accepted 28 April 2017
Available online 1 May 2017

Keywords:
Zinc oxide
Graphene
Gas sensor
Nitrogen dioxide
Metal oxide semiconductor

ABSTRACT

Hierarchical rGO/ZnO hybrids with a flower-like morphology of ZnO and flexible rGO sheets were synthesized by a facile solution-processed method. The structures and morphologies of the hybrids were investigated by different kinds of techniques, including X-ray diffraction, field-emission electron scanning microscopy, transmission electron microscopy, and energy dispersive spectroscopy. The gas sensing properties of hierarchical rGO/ZnO hybrids toward nitrogen dioxide were studied via a static system. The response of rGO/ZnO hybrids to 50 ppb NO_2 was 12, which was seven times higher than that of pristine ZnO at 100 °C. The limit of detection could be achieved as low as 5 ppb. The enhanced sensor response was attributed to the presence of local *p-n* heterojunctions between rGO sheets and hierarchical structure of ZnO.

1. Introduction

For many years, gas sensors have received considerable attention because of their important applications in detecting toxic and flammable gases, supervising air quality, and monitoring human health. Among these applications, air quality is vital to worldwide public health and future. Nitrogen dioxide (NO_2), a kind of typical air pollutant, always forms quickly from combustion emission processes in power plants and combustion engines [1,2]. In addition to contributing to the formation of ground-level ozone, acid rain and photochemical smog, NO_2 is linked with a number of adverse effects on the respiratory system [3–5]. National Ambient Air Quality Standard uses NO_2 as the indicator for the larger group of nitrogen oxides, and establishes the standard at ppb level. The requirements trigger the development of NO_2 sensors with excellent sensing properties, especially with high sensitivity.

Extensive research efforts have been committed to develop high-performance gas sensors with high sensitivity and low detection limit. Owing to their great properties such as low cost, easy synthesis, and high sensitivity, metal oxide semiconductors (MOS), involving SnO_2 [6,7], In_2O_3 [8,9], WO_3 [10,11], etc., are considered to be promising candidates for NO_2 gas sensors. To achieve desired performances of gas sensor, it is very important to make efforts in the rational design and synthesis of novel gas sensing materials. It is well known that the properties of MOS can be optimized by tailoring their morphology, size, crystal orientation, and density of defects [12]. Particularly, hierarchical nanostructures can effectively improve the gas sensing properties by increasing surface area and decreasing agglomeration [13–15].

Although many literatures suggested that the gas sensing properties could be improved through structural and morphological adjustment, this strategy is woefully inadequate for the growing requirement of the gas sensing performance. Pure single component MOS still suffers from some drawbacks arising from their limited physical or chemical characters, which will encumber their further application in high-performance gas sensors. In virtue of their tunable chemical composition and synergistic properties, heterostructured hybrids are expected to exhibit much more excellent sensing performance. MOS/carbonaceous material hybrids have been proved effective for constructing high-performance gas sensors [16–21]. Among several carbonaceous materials involving carbon nanotubes and fibers, reduced graphene oxide (rGO) as a derivative of graphene supplies more dangling bonds and active sites for gas adsorption/reaction in addition to its large surface area, these merits all contribute to the improvement of gas sensing properties.

ZnO, a well-known n-type semiconductor material, has been widely used in gas sensing application due to its good response to a variety of hazardous gases like CO, NH_3, NO_x, and volatile organic compounds (VOC) gases, low cost, and being friendly to the

* Corresponding authors.
E-mail addresses: gaoyuan@jlu.edu.cn (Y. Gao), lugy@jlu.edu.cn (G. Lu).

http://dx.doi.org/10.1016/j.snb.2017.04.190
0925-4005/

environment [22–25]. rGO/ZnO hybrids as candidates for enhancing sensing properties have been developed gradually [26–31]. For instance, sandwich-like heterostructured ZnO/graphene/ZnO made of vertically aligned ZnO nanorods arraying on double sides of graphene were synthesized for ethanol gas sensors [32]. ZnO quantum dots/graphene nanocomposites were fabricated for formaldehyde gas sensor [33]. Gas sensor based on graphene modified by atomic layer deposition ZnO film was utilized to detect formaldehyde with high sensitivity [34]. rGO-ZnO nanoparticles hybrids exhibited enhanced NO_2 sensing performances [35]. However, it remains a great challenge to improve the sensitivity of these sensors to ppb level NO_2. Being motivated by the limited research on the merging of hierarchical ZnO nanostructures with rGO and their gas sensing applications, therefore, it is of significance to develop novel hierarchical rGO/ZnO hybrids.

Herein, we presented a strategy for synthesizing hybrids with flower-like hierarchical ZnO and rGO. The approach was based on a facile and mild solution-processed method. Moreover, in comparison with pristine flower-like ZnO, the enhanced gas sensing properties of hierarchical rGO/ZnO hybrids successfully demonstrated their potential application as a superior NO_2 sensing material. The sensors based on as-prepared rGO/ZnO hybrids exhibited much more sensitivity to NO_2, and could detect NO_2 as low as 5 ppb. In addition, it showed good sensing properties in terms of selectivity, stability and response/recovery speed.

2. Experimental

2.1. Synthesis of the rGO/ZnO hybrid

All chemicals were the analytical-grade reagents and used without any other further purification. Graphene oxide (GO) was prepared by a modified Hummer's method as described in reference [36]. The rGO/ZnO material was synthesized via a conventional heating treatment using water bath with $Zn(Ac)_2{\cdot}2H_2O$ and GO as the precursors. 0.4 g $Zn(Ac)_2{\cdot}2H_2O$ powder was dissolved in 20 mL deionized water to homogeneous solution at first. Then, $NH_3{\cdot}H_2O$ was added dropwise to the solution until obtained clear solution. Afterwards, 4 mg GO was added with vigorous stirring and then the mixture was kept and heated by water bath at 80 °C for 20 min. The product was collected by centrifugation and washing several times with deionized water, and dried at −50 °C. Finally, after sintering at 350 °C for 2 h with a temperature ramp of 2 °C min^{-1}, 1.7 wt% rGO/ZnO hybrid was obtained. For comparison, rGO and bare ZnO were prepared under the same condition. All samples were freeze-dried without any treatment before characterization.

2.2. Characterization

X-ray diffraction (XRD) patterns of the as-prepared products were conducted on a Rigaku D/max-2500 X-ray diffractometer, with Cu Kα radiation (λ = 1.5406 Å). The surface morphology and microstructure of the products were observed using a JEOL JSM-7500F field emission scanning electron microscope (FESEM), which was operated at 15 kV. Transmission electron microscopy (TEM), high resolution transmission electron microscopy (HRTEM), and selected-area electron diffraction (SAED) were conducted on a JEOL JEM-3010 microscope with an accelerating voltage of 200 KV. X-ray photoelectron spectroscopies (XPS) were measured on an ESCALAB MKII X-ray photoelectron spectrometer. The specific surface area was computed using the five-point Brunauer–Emmett–Teller (BET) method by a Micromeritics Gemini VII apparatus (Surface Area and Porosity System).

2.3. Fabrication and measurement of gas sensors

Gas sensors based on the pristine ZnO and rGO/ZnO hybrid were fabricated, and the detailed fabrication procedure of sensor devices was as follows. The as-synthesized sensing material was first mixed with deionized water to form a homogeneous paste and then coated onto a ceramic tube (4 mm in length, 1.2 mm in external diameter, 0.8 mm in internal diameter), at each end of which a pair of gold electrodes had been previously installed. After the coating layer drying in air at room temperature, a Ni-Cr alloy coil was inserted into the alumina tube as a heater in order to control the working temperature of sensor. After connecting the leads to the tube base, the sensor was finally constructed. The as-produced sensors were subjected to an aging process for one week to enable stable properties.

The sensing properties of gas sensor were measured on a static system under laboratory conditions. Environmental air (30% R.H.) was used as both a reference gas. A typical testing process was as follows. Firstly, the sensor was put into the chamber of air to get a steady state, then the sensor was took to a chamber filled with the calculated amount of the tested gas or liquid diluted by air. When the response reached a constant value, transferred the sensor back to the chamber of air, and waited for recovering.

The response (S) of the gas sensor is defined as the ratio of the resistance of the sensor in the tested gases (R_g) to that in air (R_a) when tested gases are oxidative gases, that is $S = R_g/R_a$, while the tested gases are reductive gases, $S = R_a/R_g$. The response and recovery time are defined as the time taken by the sensor to achieve 90% of the total resistance variation in the case of adsorption and desorption respectively.

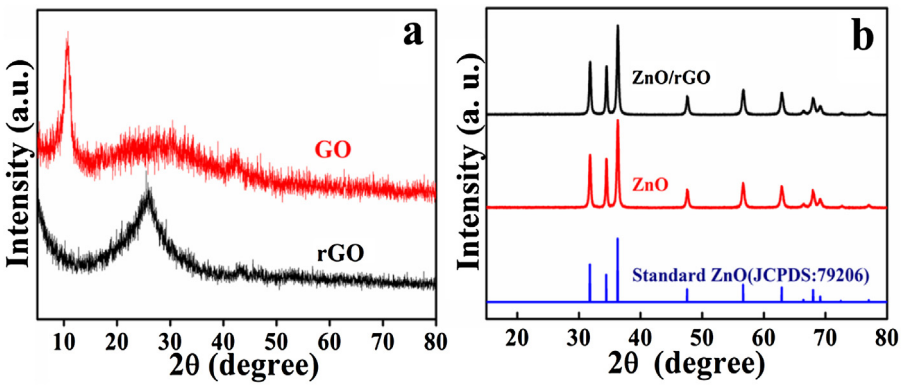

Fig 1. XRD patterns of GO and rGO (a), ZnO and 1.7% rGO/ZnO (b).

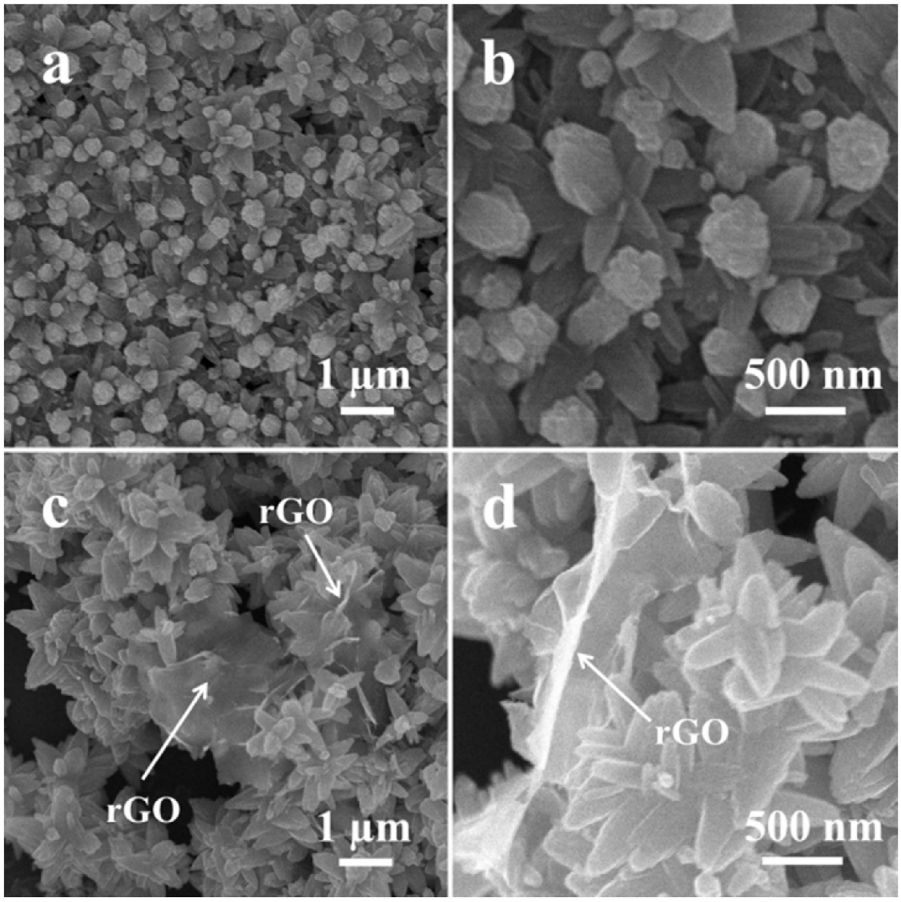

Fig. 2. FESEM images of ZnO (a, b) and 1.7% rGO/ZnO (c, d).

3. Results and discussion

3.1. Morphological and structural characteristics

Powder X-ray diffraction (XRD) was conducted to identify the composition and crystalline phase of the final products. Fig. 1 shows the typical XRD patterns of the as-synthesized GO, rGO, ZnO and rGO/ZnO hybrids. The diffraction peak at around $2\theta = 11.2^{\circ}$ in Fig. 1a belongs to the (001) reflection of GO. For the rGO sample, the characteristic diffraction peak can be observed at 23.5°, corresponding to the (002) planes of graphene [37,38]. The variation of diffraction peaks revealed successful transformation from GO to rGO via the same treatment as the synthesis of ZnO and its hybrids. All the diffraction peaks in the XRD pattern for ZnO were accorded well with those from the standard Joint Committee on Powder Diffraction Standards (JCPDS) card (No. 79-206) of the hexagonal wurtzite structure ZnO with a = 0.324 nm and c = 0.521 nm. Moreover, no other diffraction peaks derived from other crystalline phase were found. It is demonstrated that the rGO decoration process did not deteriorate the original crystal structure of pristine ZnO since all diffraction peaks of ZnO phase in the rGO/ZnO hybrids existed at almost the same 2θ position as that of the pristine ZnO. However, no obvious diffraction peaks were derived from rGO. It is probably because of the small content of rGO and the weak diffraction peaks intensity of rGO itself [39,40].

The morphologies of the samples were investigated by FESEM. Fig. 2 shows typical FESEM images of ZnO and rGO/ZnO hybrid at different magnifications. In the SEM image of ZnO (Fig. 2a), nanorods-bundled assembly structure with flower-like morphology could be observed. The high-magnification SEM image indicates that the bundles-like petals have an average length of about 500 nm. When rGO was added to hybrid with ZnO, we could observe flexible rGO sheets covered on the surface of ZnO or mixed among ZnO flowers with visible edges in Fig. 2c, d. ZnO in hybrid still assembled to flower-like hierarchical structure, and the size of flower approximated pristine ZnO. However, the addition of rGO resulted in loose ZnO petals in partial location, which assembled by less nanorods. It is obvious that the graphene additive in the experiment had the ability to affect the morphologies of as-synthesized ZnO products to an extent. The morphology and structure of rGO/ZnO were further characterized with TEM (Fig. 3a), which were in good accordance with the FESEM images. We could observe flexible rGO sheets decorated on the flower-like ZnO. Fig. 3b presents the HRTEM image of rGO/ZnO, it can be seen that the fringe lattices at the interface between two components and the adjacent lattice interplanar spacing of ZnO was 0.16 nm, corresponding to the (110) planes of the wurtzite ZnO.

The surface composition and element analysis for the as-prepared products were characterized by XPS. As shown in Fig. 4a, the XPS spectra of GO and rGO/ZnO both reveal two peaks at 285 and 530 eV, corresponding to C 1 s and O 1s, respectively. Note that rGO/ZnO hybrids exhibit several bands associated with Zn 2p, Zn 3s, Zn 3p and Zn 3d bands, which further confirms the presence of Zn element in the final hybrid samples. Additionally, the Zn $2p_{1/2}$ and $2p_{3/2}$ bands in rGO/ZnO spectrum attribute to the binding energies 1042 eV and 1019 eV, respectively, suggesting the presence of ZnO nanostructure [41]. The high-resolution C1 s XPS spectra of GO and rGO/ZnO (Fig. 4b, c) show peaks at 284.6, 286.6 and 288.4 eV, accounting for the C—C, C—O and C=O [42]. In contrast, the peak intensity of C—O and C=O in rGO/ZnO

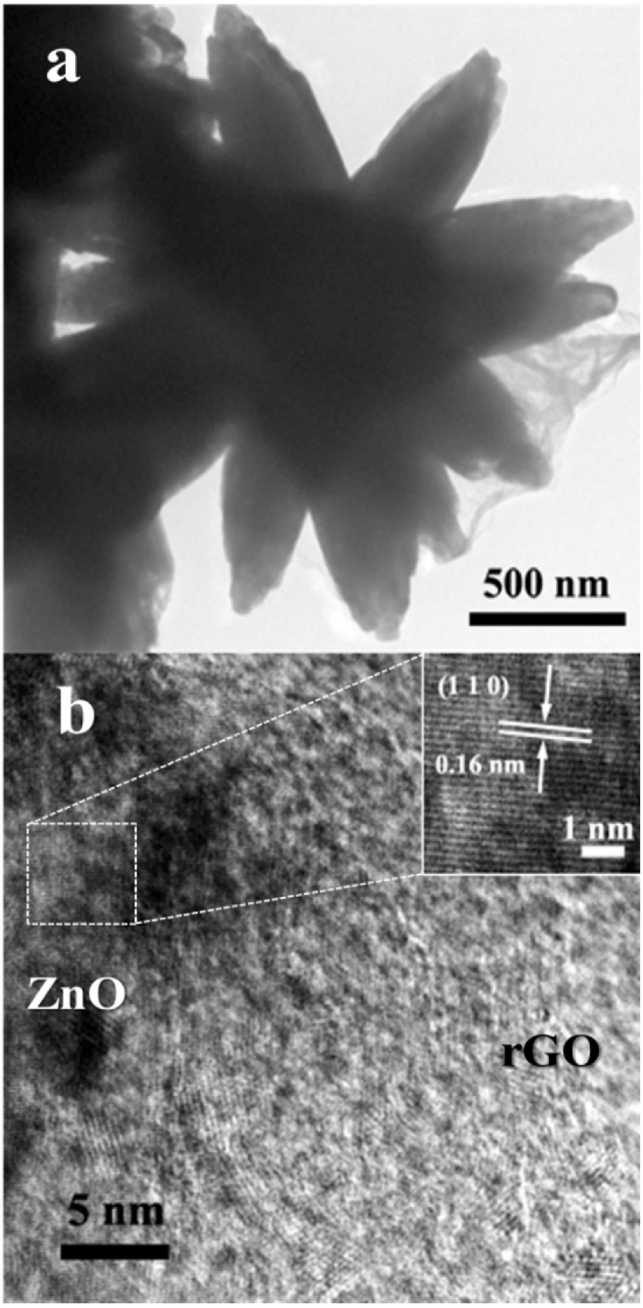

Fig. 3. Typical TEM image (a), HRTEM image (b) of 1.7% rGO/ZnO hybrid.

tremendously decreased, and the content of C—C correspondingly increased dramatically. The results suggested that most oxygen containing groups were removed during the hydrothermal treatment, leading to the successful transformation from GO to rGO. All these observations further confirm that rGO/ZnO hybrids have been successfully prepared.

The Raman spectra of GO and rGO are illustrated in Fig. 5. It is obviously seen that the samples exhibit two major peaks, containing the D band at1354 cm^{-1} and the G band at 1603 cm^{-1}. Furthermore, the intensity ratio of the D to the G band (I_D/I_G) for rGO (0.99) is higher than that for GO (0.93). The I_D/I_G customarily acts as a parameter to evaluate the disorder and defect degree of various carbon materials, that is, the higher ratio of I_D/I_G account for the higher degree of disordering in the carbon materials [43]. Given the fact that the higher I_D/I_G of rGO, we could demonstrate that new graphitic domains for rGO were formed, in other words, the GO sheets were cut into smaller ones with more edge defects during the synthesis process.

The specific surface areas of the as-obtained samples were also estimated (shown in Fig. 6), which presented that flower-like ZnO hierarchical nanostructure modified by reduced graphene oxide possess a little smaller BET surface areas (13.1 g/m^2) compared with pure ZnO (14.2 g/m^2).

3.2. Gas-sensing properties to NO_2

The gas sensing mechanism of a MOS-based sensor can be described in terms of gases adsorption/reaction on the surfaces of the sensing materials [33,44]. When the sensor is exposed in air, oxygen molecules in air are chemisorbed on the surface and form adsorbed oxygen species (O_2-, O^-, or O^{2-}). In the process, electrons are captured from the oxide conduction band, therefore an electron depletion layer with less concentration of free electrons forms at the surface of ZnO and the resistance increases consequently. While the sensor is exposed to NO_2 gas, the NO_2 molecules contact with and then adsorb at the surface of ZnO. Consequently, NO_2 molecules can not only capture electrons from the conduction band but also react with the adsorbed oxygen species, as illustrated as follows [45,46]:

$$NO_2(gas) + e^- \leftrightarrow NO_2{}^-(ads) \quad (1)$$

$$NO_2\,(gas) + O_2^-\,(ads) \leftrightarrow NO_2^-\,(ads) + O_2\,(gas) \quad (2)$$

$$O_2\,(gas) + e^- \leftrightarrow O_2^-\,(ads) \quad (3)$$

The electron extraction in these process leads to an increase in the resistance, which can be used for the detection of NO_2 gas. Furthermore, the hierarchical morphology facilitates the adsorption and diffusion of gas molecules around the active surface.

In the rGO/ZnO hybrids, the local p–n heterojunctions formed between the n-type ZnO and the p-type rGO display significant effects on the sensing performance of rGO/ZnO. The Fermi energy of ZnO is supposed to be lower than that of rGO, with the work functions of *n*-ZnO and rGO being about 5.20 and 4.75 eV [47]. The p-type rGO acts as an electron acceptor to extract electron from ZnO surface to equate the Fermi level [27,48], which results in the less electrons at ZnO surface and interface, and in turns leading to higher potential barriers and the wider depletion layer. As a result, when exposed to NO_2 atmospheres, potential barriers will further increased and depletion layer will further widened. Compared with the pristine ZnO, even same electrons transferred to the hybrids surface would lead to a larger variation in resistance and bring about enhanced sensor response. Based on the above assumption, the enhanced sensitivity to NO_2 gas would be obtained by rGO/ZnO sensor, which is attributed to the formation of local *p-n* junctions. As expected, our as-prepared hybrids showed excellent NO_2 sensing properties. The investigation was illustrated as below.

In order to demonstrate the potential application in gas sensing, gas sensors based on the rGO/ZnO were fabricated and a series of gas-sensing tests carried out to evaluate its sensing performances. It is well known that the response of a gas sensor is highly affected by the working temperature, hence, the relationships between the working temperature and gas sensing properties of the sensors based on 1.7 wt% rGO/ZnO and bare ZnO to 50 ppb NO_2 were firstly tested, and the results are shown in Fig. 7. The response of tested sensors varied with working temperature and exhibited a temperature-dependent feature. As can be seen in Fig. 7a, the sensor based on rGO/ZnO hybrid shows an enhanced response at each tested temperature in comparison to the pristine ZnO. The maximum response of rGO/ZnO hybrids could reach to 12 at the optimal working temperature of 100 °C, which was about seven times higher than that of ZnO. The temperature-dependent response time and recovery time of the sensors are also provided in Fig. 7 b and

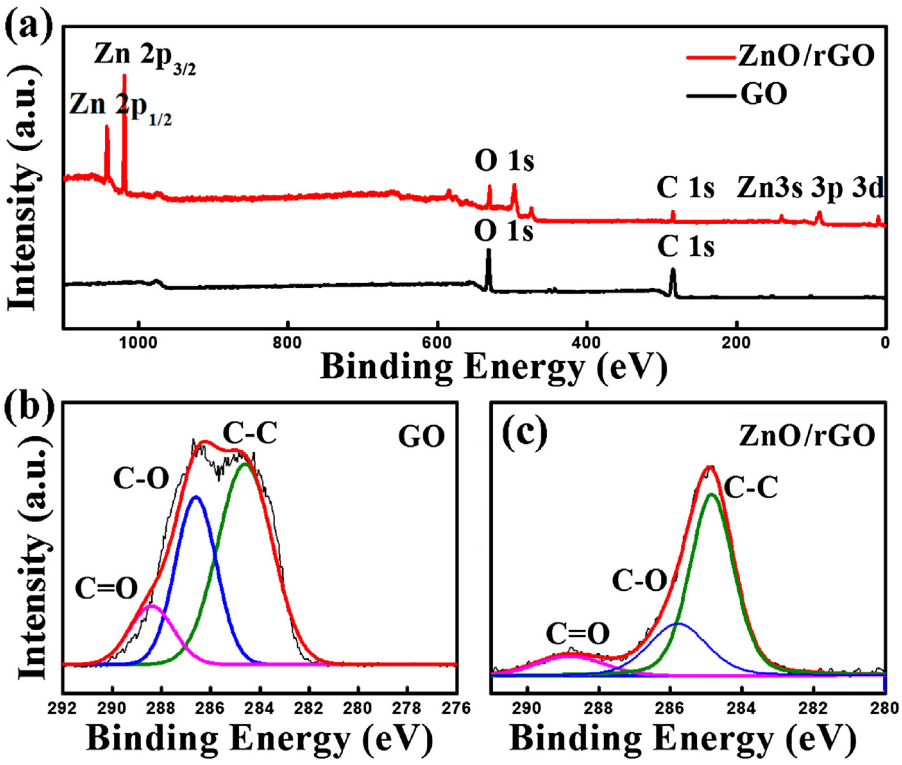

Fig. 4. XPS survey spectra of GO and 1.7% rGO/ZnO hybrid (a). C1 s spectra of GO (b) and 1.7% rGO/ZnO.

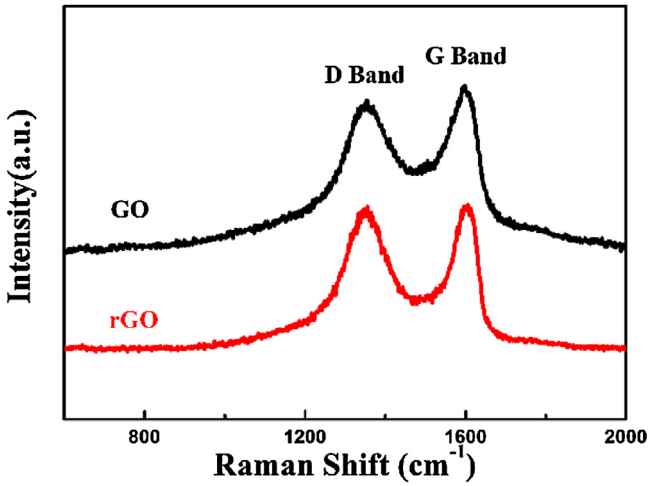

Fig. 5. The Raman spectra of GO and rGO.

c. It is clearly to see that the response time and recovery time of both sensors decreased with the increase in working temperature. Working temperature is a key factor affecting reaction rate, which seriously influences gas-adsorption/desorption process, and in turn has a great effect on response/recovery time. The same decrease trends of response/recovery time have been reported in many works based on ZnO material to detect NO_2 as ours [49–53]. The response time and recovery time of rGO/ZnO were both shorter than those of ZnO at each temperature. The result demonstrated that response time and recovery time were further reduced via introducing rGO into sensing materials. The optimal working temperature for the response of sensor based on rGO/ZnO, 100 °C, also befitted for the response time and recovery time, because those both first decreased sharply with the temperature, up to 100 °C, the decline turned to slowly. Thus, further gas sensing researches based on rGO/ZnO were conducted at the optimum working temperature of 100 °C.

The dynamic transients of a series of samples at 100 °C are shown in Fig. 8, including rGO/ZnO hybrids, ZnO and rGO. It is well known that ZnO is a classic n-type semiconductor that exhibits increased resistance in oxidizing gas, such as NO_2. Instead, p-type semiconductor, such as rGO, owing to oxygen doping, shows decreased resistance in oxidizing atmosphere. As the results shown, 1.7, 10, 15 wt% rGO/ZnO and pure ZnO displayed the increased resistance upon exposed to 50 ppb NO_2, exhibiting n-type semiconductor behavior. However, the transition from n-type to p-type had appeared when the rGO mass ratio reached 20 wt%. 20 wt% rGO/ZnO became almost unresponsive to 50 ppb NO_2 and showed decreased resistance towards 500 ppb NO_2, which is p-type semiconductor behavior. Besides transition behavior from n-type to p-type, rGO mass ratios also had an effect on the sensor response. The sensor response of samples decreased with increase in rGO mass ratio. 1.7 wt% rGO/ZnO showed the highest sensor response. Considering in the case of 1.7 wt% rGO/ZnO sample, it had a little mass ratio of rGO and exhibited n-type semiconductor behavior. Thus, we think ZnO was dominant in the hybrid for NO_2 sensing. As literatures reported, the addition of rGO could enhance the sensitivity, which is attributed to two reasons: 1) improvement of the specific surface area, 2) the formation of local *p-n* heterojunctions in the interface between ZnO and rGO [54,55]. The specific surface areas of the samples were estimated using the BET, and the results demonstrated the surface areas are 14.2 and 13.1 m^2g^{-1} for ZnO and rGO/ZnO respectively. The addition of rGO has no positive effect on the surface area. Thus, we think the formation of local *p-n* junctions between p-type rGO and n-type ZnO is the main reason for promotion of sensing performance, because it could modulate the space-charged layers at the interfaces between rGO and metal oxides. When rGO mass ratio is further increased, rGO will cover the surface active sites to hinder the reaction between gas and sur-

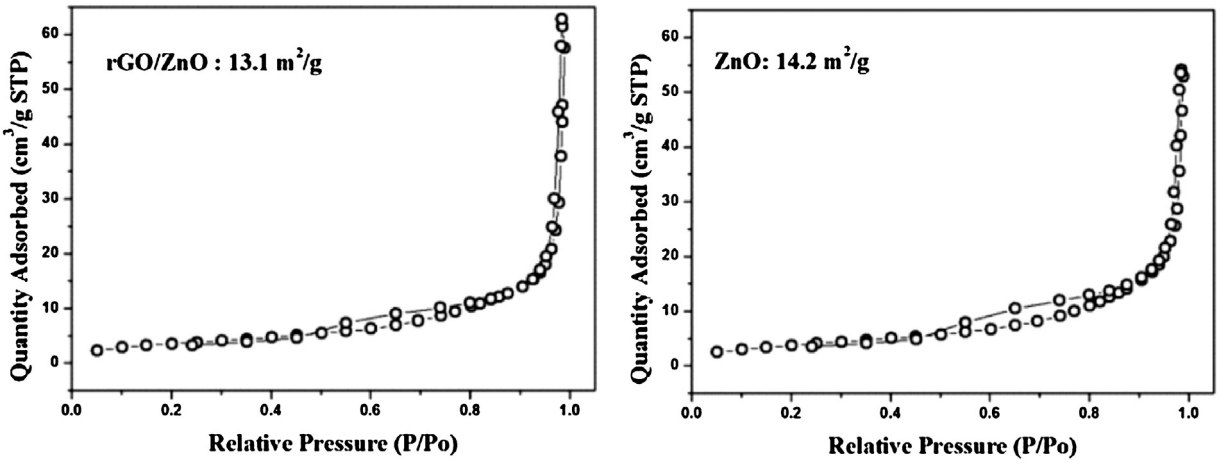

Fig. 6. The nitrogen adsorption–desorption isotherms of 1.7% rGO/ZnO hybrid (a) and prestine ZnO (b).

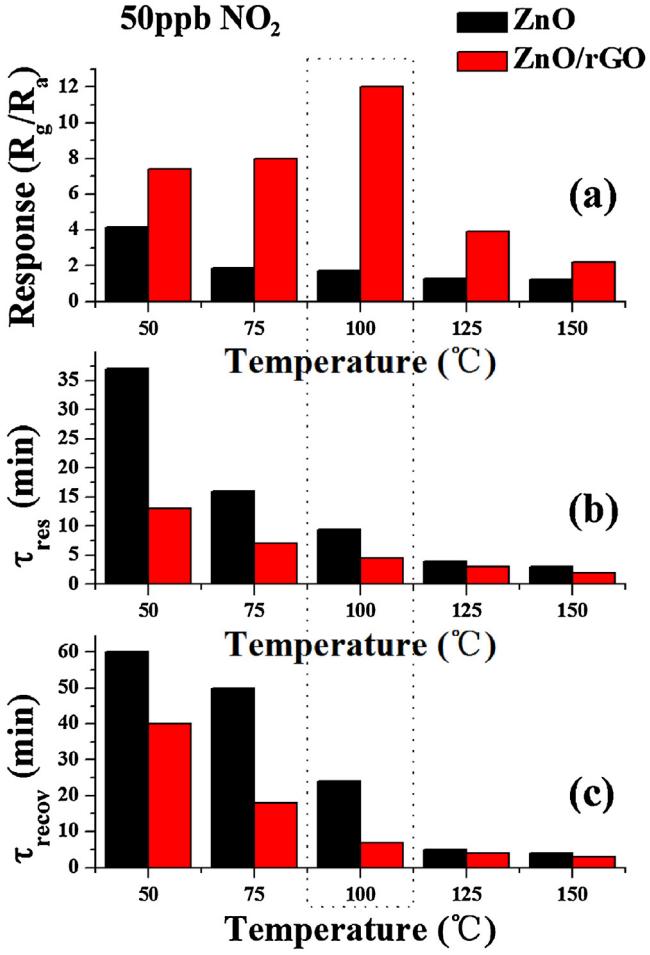

Fig. 7. Sensing properties involving sensor response (a), response time (b) and recovery time (c) of sensors based on 1.7% rGO/ZnO hybrid and pure ZnO to 50 ppb NO_2 as a function of the working temperature.

face adsorbed oxygen species, leading to the decrease in sensor response and the transition from n-type to p-type.

Fig. 9a displays the dynamic response–recovery curves of the 1.7% rGO/ZnO hybrid when orderly exposed to low-concentration NO_2 ranging from 5 to 500 ppb at 100 °C. It can be found that the resistance increased immediately when the sensor was exposed to NO_2 and then reached a steady state gradually. Soon afterwards,

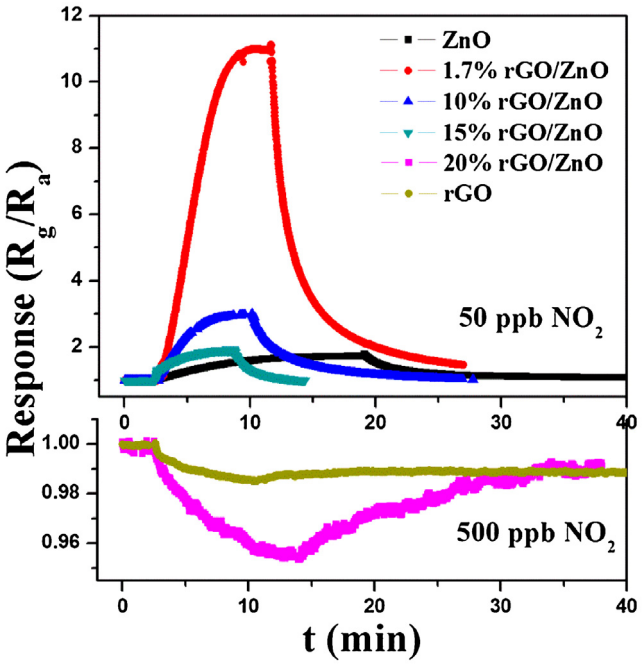

Fig. 8. The dynamic response of samples to NO_2 at 100 °C. 1.7%, 10%, 15% rGO/ZnO hybrids and ZnO toward 50 ppb NO_2; 15% rGO/ZnO hybrid and rGO toward 500 ppb NO_2.

the resistance dropped to the initial value without obvious shift when sensor was transferred back into ambient air to recover. The corresponding responses of the sensors were highly dependent on the concentration of NO_2, and showed an approximately linear increasing trend in the range of 5 ppb to 500 ppb (the inset in Fig. 9a). The linear correlation coefficient is 0.97. Apparently, when the NO_2 concentration was as low as 5 ppb, the sensor response still could reach 6.7. Comparison with the response of ZnO to 50 ppb NO_2 (only 1.7), the sensor based on rGO/ZnO exhibited much lower NO_2 detection limit, which had 10-fold improvement against pristine ZnO. The results demonstrated that rGO/ZnO hybrid exhibited super-sensitivity to ultra-trace NO_2 and it could serve as a promising sensing material for trace NO_2 detection. The time taken in the response or recovery process was also related with NO_2 concentration, however, the difference was not tremendous, as shown in Fig. 9b. The response time were about 4.3, 5.1, 5.5 min towards 500, 50, and 5 ppb NO_2, respectively. Meanwhile, their respective recovery times were around 4.8, 7.5 and 7.9 min. Despite

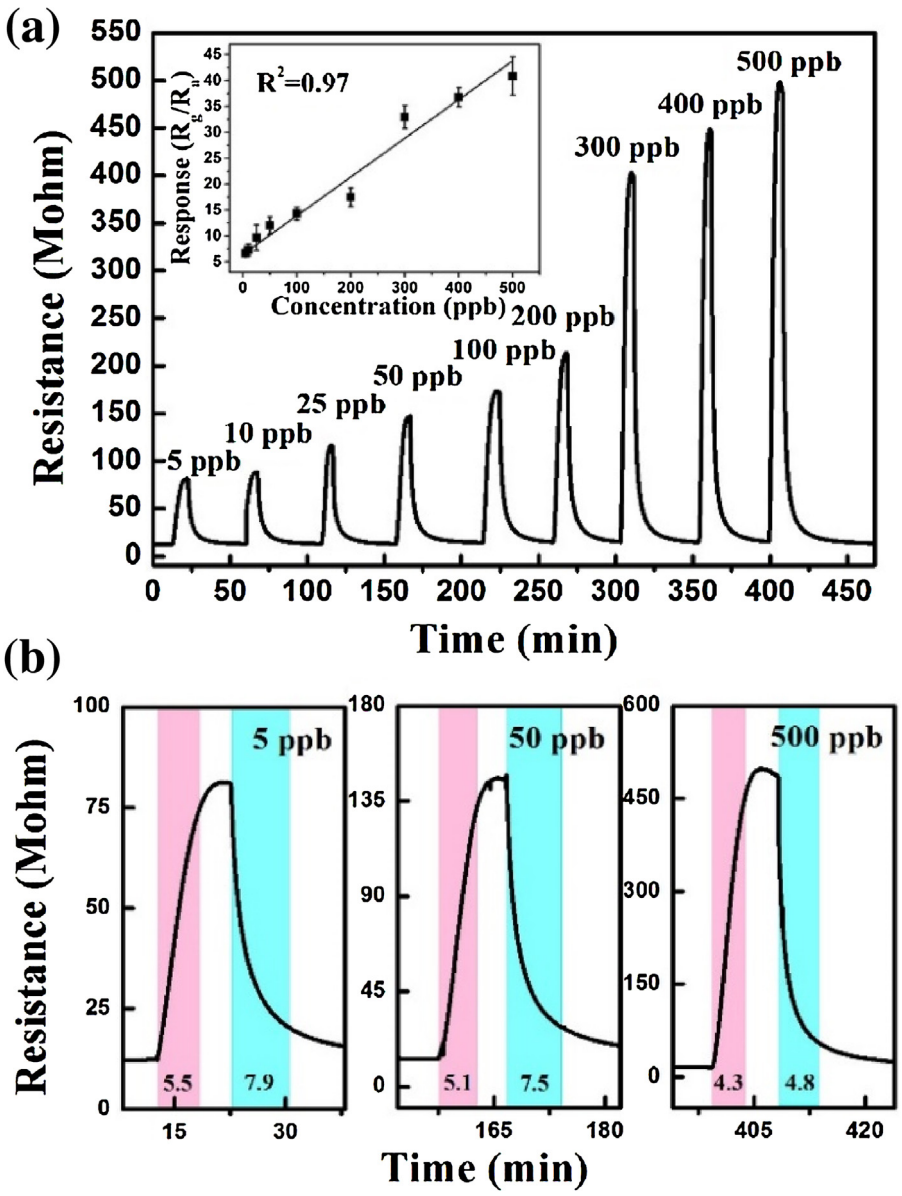

Fig. 9. Transient response of sensor based on 1.7% rGO/ZnO at 100 °C to NO_2 with different concentrations. The inset in (a) is the relationship between response and NO_2 concentration. The pink and light blue region in (b) are corresponding to response time and recovery time. (For interpretation of the references to colour in this figure legend, the reader is referred to the web version of this article.)

as general results, the response/recovery time prolongs with the decrease in tested gas concentration, our sensor exhibited good response/recovery speed to NO_2 at ppb level.

The stability of the sensor towards ultra-trace NO_2 was also investigated. It can be observed from Fig. 10 that the sensor maintains its initial response amplitude without a clear attenuation and shift when it is alternately exposed to air and 10 ppb NO_2 through five continuous response/recovery cycles, and has an approximate response/recovery time. The results indicated that the sensor exhibited a good stability and reproducibility.

The selectivity of the sensor was also studied, and the results as shown in Fig. 11 illustrated the cross-responses of the sensor towards various testing gases, including SO_2, CO_2, NH_3, methane, ethylene, methanol and ethanol. All of the gases were tested at 100 °C with a much higher concentration (at least 200-fold) against NO_2. The responses of the sensor to other various testing gases did not exceed 3.6, while the response to 50 ppb NO_2 was 12, which indicated that the sensors based on rGO/ZnO possessed good selectivity to NO_2.

The effect of environmental humidity on the response of the sensor based rGO/ZnO towards 50 ppb NO_2 at 100 °C was studied, and the results are shown in Fig. 12. The sensor response decreased with increase in ambient relative humidity. Under ambient 40% relative humidity, the response sharply drops to ~80% compared with that under 30% relative humidity. However, the variations of sensor response were no longer significant under further elevated humidity, the response just decreased to 77% when humidity was 100% R.H.

A comparison between the sensing performances of the rGO/ZnO sensor fabricated in this work and literature reports for NO_2 detection is summarized in Table 1 [30,35,56,57]. It can be clearly seen that our gas sensor based on rGO/ZnO exhibited relatively higher NO_2 response to lower concentration of NO_2 (ppb level) and the lowest detection limit than those reported in the literatures, although our sensor did not work at room temperature.

Table 1
The sensing performance comparison of different rGO/ZnO hybrids towards NO_2.

Synthesis method	Optimum working temperature (°C)	Sensing properties			References
		NO_2 concentration (ppm)	Response	Detection limit	
Solvothermal	RT	5	1.256	5 ppm	[35]
Electrospinning	400	5	≈110	1 ppm	[56]
Solvothermal	RT	50	1.08	50 ppm	[30]
Thermal evaporation with CVD	RT	100	1.174	10 ppm	[57]
Hydrothermal	100	10 ppb	12	5 ppb	Present work

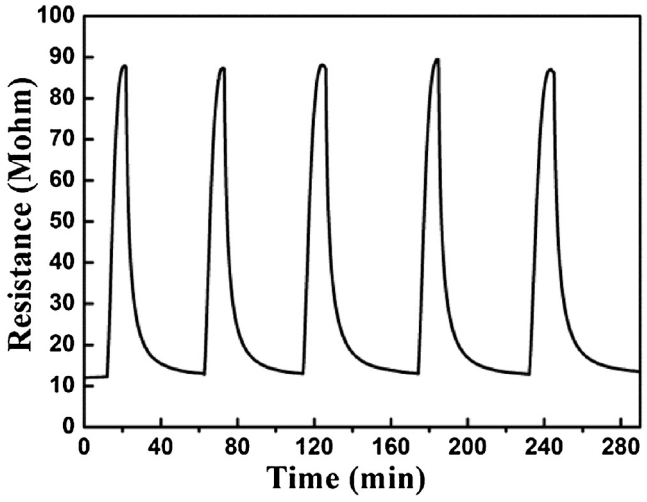

Fig. 10. The reproducibility of temporal response of 1.7% rGO/ZnO hybrid to 10 ppb NO_2 at 100 °C.

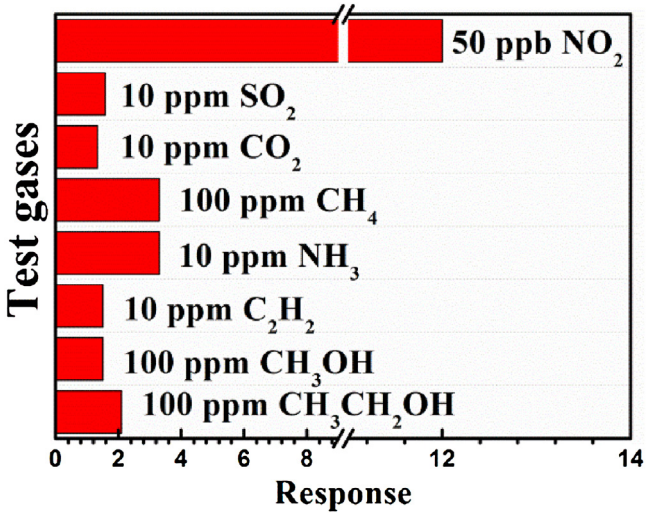

Fig. 11. The response of sensor based on 1.7% rGO/ZnO hybrid to various gases at 100 °C.

As far as we know, its excellent gas response holds overwhelming superiority in gas sensors those based on graphene/metal oxide hybrid including not only rGO/ZnO but also other metal oxide hybrids.

4. Conclusions

In summary, uniform hybrids with flower-like hierarchical ZnO and rGO have been successfully prepared by solution-processed method under mild condition. The obtained products were applied to sensor devices and their gas sensing properties were examined.

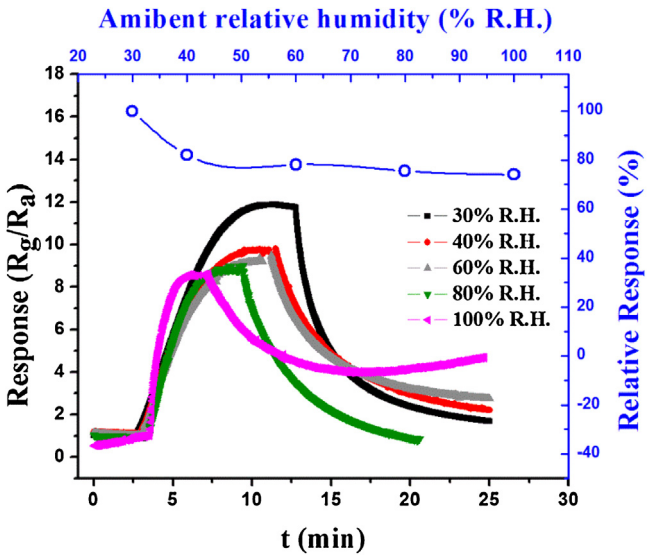

Fig. 12. Effect of ambient relative humidity on the response of sensor based on 1.7% rGO/ZnO exposed to 50 ppb NO_2 at 100 °C.

It was found that the device based on 1.7 wt% rGO/ZnO exhibited an ultralow detection limit (5 ppb) and a higher response toward NO_2 in comparison to the pristine flower-like ZnO architecture, which have confirmed the potential of rGO/ZnO hybrids for gas sensing applications. Moreover, the enhanced sensing performances have been demonstrated to be related to their unique hierarchical architecture andthe local heterojunctions in hybrids.

Acknowledgement

This work was supported by the National Nature Science Foundation of China (61304242, 61327804, 61377058 and 61374218), National High-Tech Research and Development Program of China (863 Program, No. 2014AA06A505), Science and Technology Development Program of Jilin Province (No.20150520091JH).

References

[1] W. Yang, S.T. Omaye, Air pollutants, oxidative stress and human health, Mutat. Res.-Gen. Tox. En. 674 (2009) 45.
[2] R. Moos, B. Reetmeyer, A. Hürland, C. Plog, Sensor for directly determining the exhaust gas recirculation rate—EGR sensor, Sens. Actuators B: Chem. 119 (2006) 57.
[3] A. Malik, R. Tauler, Exploring the interaction between O3 and NOx pollution patterns in the atmosphere of Barcelona, Spain using the MCR-ALS method, Sci. Total Environ. 517 (2015) 151.
[4] F. Cibella, G. Cuttitta, R. Della Maggiore, S. Ruggieri, S. Panunzi, A. De Gaetano, S. Bucchieri, G. Drago, M.R. Melis, S. La Grutta, G. Viegi, Effect of indoor nitrogen dioxide on lung function in urban environment, Environ. Res. 138 (2015) 8.
[5] C. Marichy, P.A. Russo, M. Latino, J.-P. Tessonnier, M.-G. Willinger, N. Donato, G. Neri, N. Pinna, Tin dioxide-Carbon heterostructures applied to gas sensing: structure-Dependent properties and general sensing mechanism, J. Phys. Chem. C 117 (2013) 19729.

[6] S.-W. Choi, A. Katoch, G.-J. Sun, P. Wu, S.S. Kim, NO2-sensing performance of SnO2 microrods by functionalization of Ag nanoparticles, J. Mater. Chem. C 1 (2013) 2834.
[7] M. Epifani, J.D. Prades, E. Comini, E. Pellicer, M. Avella, P. Siciliano, G. Faglia, A. Cirera, R. Scotti, F. Morazzoni, J.R. Morante, The role of surface oxygen vacancies in the NO2 sensing properties of SnO2 nanocrystals, J. Phys. Chem. C 112 (2008) 19540.
[8] M. Ivanovskaya, A. Gurlo, P. Bogdanov, Mechanism of O3 and NO2 detection and selectivity of In2O3 sensors, Sens. Actuators B: Chem. 77 (2001) 264.
[9] S.P. Patil, V.L. Patil, S.S. Shendage, N.S. Harale, S.A. Vanalakar, J.H. Kim, P.S. Patil, Spray pyrolyzed indium oxide thick films as NO2 gas sensor, Ceram. Int. 42 (2016) 16160.
[10] X. An, J.C. Yu, Y. Wang, Y. Hu, X. Yu, G. Zhang, WO3 nanorods/graphene nanocomposites for high-efficiency visible-light-driven photocatalysis and NO2 gas sensing, J. Mater. Chem. 22 (2012) 8525.
[11] Z. Wang, P. Sun, T. Yang, Y. Gao, X. Li, G. Lu, Y. Du, Flower-like WO3 architectures synthesized via a microwave-assisted method and their gas sensing properties, Sens. Actuators B: Chem. 186 (2013) 734.
[12] C. Yujin, Z. Chunling, W. Taihong, The enhanced ethanol sensing properties of multi-walled carbon nanotubes/SnO 2 core/shell nanostructures, Nanotechnology 17 (2006) 3012.
[13] J.-H. Lee, Gas sensors using hierarchical and hollow oxide nanostructures: overview, Sens. Actuators B: Chem. 140 (2009) 319.
[14] H.-J. Kim, J.-W. Yoon, K.-I. Choi, H.W. Jang, A. Umar, J.-H. Lee, Ultraselective and sensitive detection of xylene and toluene for monitoring indoor air pollution using Cr-doped NiO hierarchical nanostructures, Nanoscale 5 (2013) 7066.
[15] S.-J. Hwang, K.-I. Choi, J.-W. Yoon, Y.C. Kang, J.-H. Lee, Pure and palladium-Loaded Co3O4 hollow hierarchical nanostructures with giant and ultraselective chemiresistivity to xylene and toluene, Chem. Eur. J. 21 (2015) 5872.
[16] S. Cui, H. Pu, G. Lu, Z. Wen, E.C. Mattson, C. Hirschmugl, M. Gajdardziska-Josifovska, M. Weinert, J. Chen, Fast and selective room-Temperature ammonia sensors using silver nanocrystal-Functionalized carbon nanotubes, ACS Appl. Mat. Interfaces 4 (2012) 4898.
[17] A. Sharma, M. Tomar, V. Gupta, Room temperature trace level detection of NO2 gas using SnO2 modified carbon nanotubes based sensor, J. Mater. Chem. 22 (2012) 23608.
[18] Q. Vu Van, D. Nguyen Van, T. Ngo Sy, H. Nguyen Duc, D. Nguyen Van, H. Nguyen Van, Outstanding gas-sensing performance of graphene/SnO2 nanowire Schottky junctions, Appl. Phys. Lett. 105 (2014).
[19] J.S. Lee, O.S. Kwon, D.H. Shin, J. Jang, WO3 nanonodule-decorated hybrid carbon nanofibers for NO2 gas sensor application, J. Mater. Chem. A 1 (2013) 9099.
[20] S. Cui, Z. Wen, E.C. Mattson, S. Mao, J. Chang, M. Weinert, C.J. Hirschmugl, M. Gajdardziska-Josifovska, J. Chen, Indium-doped SnO2 nanoparticle-graphene nanohybrids: simple one-pot synthesis and their selective detection of NO2, J. Mater. Chem. A 1 (2013) 4462.
[21] F. Liu, X. Chu, Y. Dong, W. Zhang, W. Sun, L. Shen, Acetone gas sensors based on graphene-ZnFe2O4 composite prepared by solvothermal method, Sens. Actuators B: Chem. 188 (2013) 469.
[22] J.-Q. He, J. Yin, D. Liu, L.-X. Zhang, F.-S. Cai, L.-J. Bie, Enhanced acetone gas-sensing performance of La2O3-doped flowerlike ZnO structure composed of nanorods, Sens. Actuators B: Chem. 182 (2013) 170.
[23] C.W. Na, S.-Y. Park, J.-H. Lee, Punched ZnO nanobelt networks for highly sensitive gas sensors, Sens. Actuators B: Chem. 174 (2012) 495.
[24] K.-M. Kim, H.-R. Kim, K.-I. Choi, H.-J. Kim, J.-H. Lee, ZnO hierarchical nanostructures grown at room temperature and their C2H5OH sensor applications, Sens. Actuators B: Chem. 155 (2011) 745.
[25] J. Choi, H. Ji, O.T. Tambunan, I.-S. Hwang, H.-S. Woo, J.-H. Lee, B.W. Lee, C. Liu, S.J. Rhee, C.U. Jung, G.-T. Kim, Brush-Shaped ZnO heteronanorods synthesized using thermal-Assisted pulsed laser deposition, ACS Appl. Mat. Interfaces 3 (2011) 4682.
[26] G. Singh, A. Choudhary, D. Haranath, A.G. Joshi, N. Singh, S. Singh, R. Pasricha, ZnO decorated luminescent graphene as a potential gas sensor at room temperature, Carbon 50 (2012) 385.
[27] X. Yu, G. Zhang, H. Cao, X. An, Y. Wang, Z. Shu, X. An, F. Hua, ZnO@ZnS hollow dumbbells-graphene composites as high-performance photocatalysts and alcohol sensors, New J. Chem. 36 (2012) 2593.
[28] P. Afzali, Y. Abdi, E. Arzi, Directional reduction of graphene oxide sheets using photocatalytic activity of ZnO nanowires for the fabrication of a high sensitive oxygen sensor, Sens. Actuators B: Chem. 195 (2014) 92.
[29] K. Anand, O. Singh, M.P. Singh, J. Kaur, R.C. Singh, Hydrogen sensor based on graphene/ZnO nanocomposite, Sens. Actuators B: Chem. 195 (2014) 409.
[30] X. Liu, J. Sun, X. Zhang, Novel 3D graphene aerogel?ZnO composites as efficient detection for NO2 at room temperature, Sens. Actuators B: Chem. 211 (2015) 220.
[31] L. Yu, H. Song, Y. Tang, L. Zhang, Y. Lv, Controllable deposition of ZnO-doped SnO2 nanowires on Au/graphene and their application in cataluminescence sensing for alcohols and ketones, Sens. Actuators B: Chem. 203 (2014) 726.
[32] R. Zou, G. He, K. Xu, Q. Liu, Z. Zhang, J. Hu, ZnO nanorods on reduced graphene sheets with excellent field emission, gas sensor and photocatalytic properties, J. Mater. Chem. A 1 (2013) 8445.
[33] Q. Huang, D. Zeng, H. Li, C. Xie, Room temperature formaldehyde sensors with enhanced performance, fast response and recovery based on zinc oxide quantum dots/graphene nanocomposites, Nanoscale 4 (2012) 5651.
[34] H. Mu, Z. Zhang, X. Zhao, F. Liu, K. Wang, H. Xie, High sensitive formaldehyde graphene gas sensor modified by atomic layer deposition zinc oxide films, Appl. Phys. Lett. 105 (2014).
[35] S. Liu, B. Yu, H. Zhang, T. Fei, T. Zhang, Enhancing NO2 gas sensing performances at room temperature based on reduced graphene oxide-ZnO nanoparticles hybrids, Sens. Actuators B: Chem. 202 (2014) 272.
[36] Y. Gao, Y. Li, L. Zhang, H. Huang, J. Hu, S.M. Shah, X. Su, Adsorption and removal of tetracycline antibiotics from aqueous solution by graphene oxide, J. Colloid Interface Sci. 368 (2012) 540.
[37] Z. Wang, Y. Xiao, X. Cui, P.i Cheng, B. Wang, Y. Gao, X. Li, T. Yang, T. Zhang, G. Lu, Humidity-Sensing properties of urchinlike CuO nanostructures modified by reduced graphene oxide, ACS Appl Mater. Interfaces 6 (2014) 3888–3895.
[38] X. Xu, Tao Wu, F. Xia, Yi Li, C.g. Zhang, L. Zhang, M. Chen, X. Li, L. Zhang, Y. Liu, J. Gao, Redox reaction between graphene oxide and In powder to prepare In2O3/reduced graphene oxide hybrids for supercapacitors, J. Power Sources 266 (2014) 282–290.
[39] F. Gu, R. Nie, D. Han, Z. Wang, In_2O_3–graphene nanocomposite based gas sensor for selective detection of NO_2 at room temperature, Sens. Actuators B 219 (2015) 94–99.
[40] X. An, J.C. Yu, Y. Wang, Y. Hu, X. Yu, G. Zhang, WO3 nanorods/graphene nanocomposites for high-efficiency visible-light-driven photocatalysis and NO2 gas sensing, J. Mater. Chem. 22 (2012) 8525–8531.
[41] V.V. Ganbavle, S.I. Inamdar, G.L. Agawane, J.H. Kim, K.Y. Rajpure, Synthesis of fast response, highly sensitive and selective Ni:ZnO based NO_2 sensor, Chem. Eng. J. 286 (2016) 36–47.
[42] W. Yang, P. Wan, X. Zhou, J. Hu, Y. Guan, L. Feng, Additive-free synthesis of In_2O_3 cubes embedded into graphene sheets and their enhanced NO_2 sensing performance at room temperature, ACS Appl. Mater. Interfaces 6 (2014) 21093–21100.
[43] S. Liu, J. Tian, L. Wang, Y. Luo, X. Sun, One-Pot synthesis of CuO nanoflower-decorated reduced graphene oxide and its application to photocatalytic degradation of dyes, Catal. Sci. Technol. 2 (2) (2012) 339–344.
[44] P. Rai, J.-W. Yoon, C.-H. Kwak, J.-H. Lee, Role of Pd nanoparticles in gas sensing behaviour of Pd@In2O3 yolk-shell nanoreactors, J. Mater. Chem. A 4 (2016) 264.
[45] G. Lu, L.E. Ocola, J. Chen, Room-temperature gas sensing based on electron transfer between discrete tin oxide nanocrystals and multiwalled carbon nanotubes, Adv. Mater. 21 (2009) 2487.
[46] L. Wang, J. Gao, B. Wu, K. Kan, S. Xu, Y. Xie, L. Li, K. Shi, Designed synthesis of In2O3 Beads@TiO2–In2O3 composite nanofibers for high performance NO2 sensor at room temperature. ACS appl. mat, Interfaces 7 (2015) 27152.
[47] Z.U. Abideen, H.W. Kim, S.S. Kim, An ultra-sensitive hydrogen gas sensor using reduced graphene oxide-loaded ZnO nanofibers, Chem. Commun. 51 (2015) 15418–15421.
[48] A.S.M.I. Uddin, G.-S. Chung, Synthesis of highly dispersed ZnO nanoparticles on graphene surface and their acetylene sensing properties, Sens. Actuators B: Chem. 205 (2014) 338.
[49] S. Öztürk, N. Kılınç, Z.Z. Öztürk, Fabrication of ZnO nanorods for NO2 sensor applications: effect of dimensions and electrode position, J. Alloys Compounds 581 (2013) 196–201.
[50] R. NISHA, K.N. Madhusoodanan, T.V. Vimalkumar, K.P. Vijayakumar, Gas sensing application of nanocrystalline zinc oxide thin films prepared by spray pyrolysis, Bull. Mater. Sci. 38 (No. 3) (2015) 583–591.
[51] P. Chou, H. Chen, I. Liu, C. Chen, J. Liou, C. Lai, W. Liu, Senior member IEEE, nitrogen oxide (NO_2) gas sensing performance of ZnO nanoparticles (NPs)/Sapphire-Based sensors, IEEE Sens. J. 15 (NO. 7) (2015) 3759–3763.
[52] B.A. Albiss, W.A. Sakhaneh, I. Jumah, I.M. Obaidat, NO_2 gas sensing properties of znO/Single-Wall carbon nanotube composites, IEEE Sens. J. 10 (NO. 12) (2010) 1807–1812.
[53] M.-W. Ahn, K.-S. Park, J.-H. Heo, D.-W. Kim, K.J. Choi, J.-G. Park, On-chip fabrication of ZnO-nanowire gas sensor with high gas sensitivity, Sens. Actuators B 138 (2009) 168–173.
[54] F. Meng, Z. Guo, X. Huang, Graphene-based hybrids for chemiresistive gas sensors, Trends in Analytical Chem. 68 (2015) 37–47.
[55] Y. Xiao, Q. Yang, Z. Wang, R. Zhang, Y. Gao, P. Sun, Y. Sun, G. Lu, Improvement of NO_2 gas sensing performance based on discoid tin oxide modified by reduced graphene oxide, Sens. Actuators B 227 (2016) 419–426.
[56] Z.U. Abideen, A. Katoch, J.-H. Kim, Y.J. Kwon, H.W. Kim, S.S. Kim, Excellent gas detection of ZnO nanofibers by loading with reduced graphene oxide nanosheets, Sens. Actuators B: Chem. 221 (2015) 1499.
[57] J. Li, X. Liu, J. Sun, One step solvothermal synthesis of urchin-like ZnO nanorods/graphene hollow spheres and their NO2 gas sensing properties, Ceram. Int. 42 (2016) 2085.

Biographies

Jie Liu received her BE degree from Jilin University of China in 2015. She is currently working toward the MS degree in the Electronics Science and Engineering department, Jilin University. Her current research is focus on the preparation and application of graphene and semiconductor oxide, especial in gas sensor.

Shan Li is presently studying the MS degree in the Electronics Science and Engineering department, Jilin University. Her research directions involve fabrication of mesoporous oxide semiconductor and their applications in gas sensors.

Bo Zhang received the BE degree in College of Chemistry from Jilin University in 2013. He is currently working toward the Dr. degree in College of Electronic Science and Engineering, Jilin University. His research interests include the synthesis of graphene and its applications.

Yan Xiao is currently working toward the MS degree in the Electronics Science and Engineering department, Jilin University. Her research interests include the synthesis of graphene functionalized metal oxide semiconductor materials and their applications in gas sensors.

Yuan Gao received her PhD degree from the Department of Analytical Chemistry at Jilin University in 2012. She is currently an associate professor in Jilin University, China. Her current research focuses on the preparation and application of graphene oxide and semiconductor oxide, especially in gas sensors and biosensors.

Qiuyue Yang received her BS degree from Electronics Science and Engineering Department, Jilin University, China in 2013. Presently, she is a graduate student, majored in microelectronics and solid state electronics.

Yinglin Wang received the MS degree in polymer chemistry and physics from Changchun University of Technology in 2014. She is currently studying for her Dr. Eng. degree in College of Electronic Science and Engineering, Jilin University. Her research interests include the synthesis of mesoporous materials and their applications in gas sensors.

Geyu Lu received the BS degree in electronic sciences in 1985 and the MS degree in 1988 from Jilin University in China and the Dr Eng degree in 1998 from Kyushu University in Japan. Now he is a professor of Jilin University, China. Now, he is interested in the development of functional materials and chemical sensors.